Available online at www.sciencedirect.com

SciVerse ScienceDirect

Ceramics International 38 (2012) 6461–6467

CERAMICS INTERNATIONAL

www.elsevier.com/locate/ceramint

# Farming of ZnO nanorod-arrays via aqueous chemical route for photoelectrochemical solar cell application

S.A. Vanalakar[a,*], S.S. Mali[b], R.C. Pawar[b], D.S. Dalavi[b], A.V. Mohalkar[b], H.P. Deshamukh[c], P.S. Patil[b,*]

[a]*Department of Science, Institute of Civil and Rural Engineering, Shree Mouni Vidhyapeeth Gargoti, Kolhapur, Maharashtra 416209, India*
[b]*Thin Film Materials Laboratory, Department of Physics, Shivaji University, Kolhapur, Maharashtra 416004, India*
[c]*Department of Physics, Y.M. College, Pune, India*

Received 23 December 2011; received in revised form 8 May 2012; accepted 8 May 2012
Available online 15 May 2012

**Abstract**

A low temperature aqueous chemical route is employed for the synthesis of zinc oxide (ZnO) nanorod arrays onto the soda lime and fluorine-doped tin oxide (FTO) coated glass substrates at various deposition times. Synthesis/farming of ZnO nanorod arrays (ZNRs) consists of the three-step as-ZnO seed forming, ZnO seed sowing followed by ZnO nanorod arrays growing. The length and diameter of ZnO nanorods increased with the reaction time prolonging. The physical, chemical and morphological properties were analyzed by means of X-ray diffraction (XRD), UV–visible spectroscopy (UV–vis), photoluminescence (PL), energy dispersive spectroscopy (EDS) and scanning electron microscopy (SEM) respectively. The XRD pattern revealed wurtzite crystal structures of ZNRs, preferentially orienting in the (002) direction. SEM micrographs show that the ZnO nanorods grew up perpendicular to the substrate and their length increases with increase in deposition time. Finally, the photoelectrochemical (PEC) performance of ZNRs thin films were studied. The junction quality factor upon illumination ($n_l$), series and shunt resistance ($R_s$ and $R_{sh}$), flat-band-potential ($V_{FB}$), fill factor ($FF$) and efficiency ($\eta$) have been estimated.


*Keywords:* Zinc oxide nanorods; Effect on nanorod length; Photoelectrochemical cells

## 1. Introduction

Zinc oxide (ZnO) is an environmentally benevolent and technologically important semiconductor material having direct band gap of 3.37 eV. It has attracted considerable attention due to its optical, electrical, and piezoelectric properties. Its exciton binding energy, (60 MeV), has been considered as a promising candidate for UV light-emitting diodes. Moreover, due to its non-centro-symmetric symmetry, it is piezoelectric, which is a key phenomenon in building electrochemical and electromechanical applications [1]. ZnO exhibits various morphologies by varying its preparative parameters. The nanostructure arrays of ZnO, including rods, disc, belts, tubes, towers, stars, dendrite and flowers, etc. have been attracting vast interest in the field of nanotechnology [2–5]. These nanostructure arrays have been successfully used in the photo-detectors, optical modulator waveguides, light-emitting diodes, gas sensors, solar cells, etc. [6–12]. Among various nanostructures, films with well-aligned ZnO nanorods exhibit much larger surface areas. Moreover, these nanorods are packed very densely, enabling the fast and effective transport of electrons.

However, it still remains a big challenge to develop simple and reliable synthetic methods for hierarchical architectures. Several techniques have been used for deposits ZnO thin films, including Chemical Vapor Deposition (CVD) [13], Spray Pyrolysis Technique (SPT) [14], Chemical Bath Deposition (CBD) [15], Electrodeposition (ED) [16], and aqueous chemical method [17,18]. Herein, the aqueous chemical route is the best option due to its simplicity, low temperature, inexpensive, able to tune surface orientation and morphology and reproducibility to deposit large area thin films [19,20]. This aqueous chemical method involves the

*Corresponding authors. Tel.: +91 231 2609230; fax: +91 231 2691533.
*E-mail addresses:* sharad.vanalakar@gmail.com (S.A. Vanalakar), psp_phy@unishivaji.ac.in (P.S. Patil).

0272-8842/$36.00 © 2012 Elsevier Ltd and Techna Group S.r.l. All rights reserved.
http://dx.doi.org/10.1016/j.ceramint.2012.05.023

condensation of vapors and return of this condensate to the system from which it originates.

In the present work, efforts were made to deposit ZnO nanorod arrays (ZNRs) with different lengths and aspect ratios onto glass and FTO coated substrates. It is possible to grow ZNRs of different dimensions simply by varying deposition times. The deposited ZNRs were analyzed for their structural, optical and surface morphological study and photo-electrochemical performance.

## 2. Materials and method

### 2.1. Materials

Zinc acetate (Zn $(CH_3COO)_2 \cdot 2H_2O$), Hexamethylenetetramine (HMTA), Diethanolamine (HN $(CH_2CH_2OH)_2$, DEA) and ethanol were purchased from s.d. fine chemicals and used without further purification.

### 2.2. Farming of ZnO nanorods

Farming of ZNRs thin film consists of the three-steps as—ZnO seed forming, ZnO seed sowing followed by ZnO nanorods growing. The seed solution was prepared in absolute ethanol with 0.05 M zinc acetate and 0.05 M diethanolamine. The cleaned glass substrate was dip coated for 10 s in a seed solution and then kept at room temperature for drying. The dried films were annealed at 400 °C for 2 min in air to yield a seed layer of ZnO. The seeded substrate was placed vertically in 200 ml solution of equimolar zinc acetate and HMTA and refluxed at $95 \pm 3$ °C for 3 h. The prepared samples were denoted as ZnO-3. In the similar way the ZnO samples were deposited at different time interval varying 6, 9 and 12 h denoted as ZnO-6, ZnO-9 and ZnO-12 respectively. The deposited films were rinsed with distilled water and allowed to dry at room temperature.

### 2.3. Characterization

The structural properties of the ZnO thin films were studied by X-ray diffraction (XRD) using an X-ray diffractometer (Philips, PW 3710, Almelo, Holland) operating at 25 kV and 20 mA with CrKα radiation (2.29 Å). The optical absorbance of ZnO thin films was recorded using a UV–visible spectrophotometer (UV3600, Shimadzu, Japan). Scanning electron microscopy (SEM) (Model JEOL-JSM-6360, Japan) operated at an accelerating voltage of 20 kV was used to analyze the morphology of the ZNRs films. The energy dispersive spectroscopic (EDS) analysis was investigated by SEM coupled with an energy dispersive spectroscopy (EDS) unit. The thickness of the resulting ZnO thin films was estimated using a surface profiler (Ambios XP-1) and also from cross section SEM images. The room temperature photoluminescence was recorded by using JASCO F.P.-750 Model, (Japan) spectrofluorometer with excitation energy 317 nm using 1000 W Xenon lamp. The scanning speed was 1200 nm/min, the PMT voltage 700 V and the width of excitation slit and emission slit 10 nm.

The photoelectrochemical (PEC) performance was studied by semiconductor characterization system (SCS-4200 Keithely, Germany) using two electrode configurations. The ZNRs films (active area 1 $cm^2$) and graphite (active area 1 $cm^2$) were employed as the working and counter electrodes, respectively. The distance between the photoelectrode and counter electrode was 0.5 cm. An aqueous 0.5 M $Na_2SO_4$ solution was used as the redox electrolyte. The experiments were performed under SUNLUX 500/250 V UV light, intensity of 5 m $Wcm^{-2}$. Measurements of the power output characteristics and $J$–$V$ plots were made at fixed intervals after waiting a sufficient amount of time for the system to reach equilibrium (both in the dark and under illumination). A plot of $\log J$ vs $V$ was used to calculate the junction ideality factor in dark. Capacitance–voltage ($C$–$V$) characteristics were measured with respect to saturated calomel electrode (SCE) as a reference electrode. The flat-band potential ($V_{fb}$) is estimated by extrapolating the $C^{-2}$ vs $V$ (with respect to SCE).

## 3. Results and discussion

Farming of ZNRs thin film consists of the three-steps. The first one is the ZnO seed forming or nucleation, which initiates the growth of low-dimensional nanostructures. The seeded films served as nucleation sites and also provided a preferential crystallographic growth direction to the resulting nanorods. The second step is the growth, and for one-dimensional structure it is important to achieve anisotropic growth with good control over size, shape and orientation. In the present experiment, zinc-diacetae-dihydrate is converted into zinc-acetate ion (cation), acetate ion, photon and hydroxy anion.

$$H_3C-\overset{O-H-OH}{\overset{\|}{C}}-O-Zn-\overset{O-H-OH}{\overset{\|}{O}}-C-CH_3 \longrightarrow [CH_3-\overset{O}{\overset{\|}{C}}-O-Zn]^+ + [O-\overset{O}{\overset{\|}{C}}-CH_3] + 2H^+ + 2OH^-$$

The product which is obtained in the above reaction is again converted into acetic acid and zinc hydroxide. When this solution was heated the ionic product exceeds the solubility product and precipitation occurred on the substrate and in the solution to form ZnO nuclei.

$$[CH_3-\overset{O}{\overset{\|}{C}}-O-Zn]^+ + 2H^+ + 2OH^- \longrightarrow CH_3COOH + Zn(OH)_2$$

These $Zn(OH)_2$ transform to ZnO by removing of water molecules. These ZnO species form a ZnO seed. These ZnO seeds agglomerated together to form a hexagonal planar nucleus. The structure of ZnO wurtzite crystal can be described as a number of alternating planes composed of $Zn^{2+}$ ions tetrahedrally coordinated with four $O^{2-}$ ions and, stacked along the *c*-axis. This one face of the hexagonal sheet is Zn rich and forms the positively charged (002) planes whereas the opposite face is negatively charged O-(00−2) plane. Due to this reason, the Zn rich positive (002) surface being more reactive than the oxygen rich negative (002) surface and can attract new ZnO species or the opposite ionic species to its surface. In this experiment, surfactant like HMTA plays an important role in controlling the lateral growth of the nanorods. The surfactant molecules at a higher concentration are believed to form rod-like micelles. It is known that HMTA is a highly water soluble, non-ionic tetradentate cyclic tertiary amine, which provides $OH^-$ ions for the crystallization of ZnO and forms ligand with $Zn^{2+}$ in the solution. It also modifies the non-polar facets of zincite crystal and provides the vertical growth along (002) plane. These vertical growth is stable at low temperature and during the period of deposition, the $Zn(OH)_2$ molecules within the micelles begin to decompose. Also, the elevated temperature may have increased the activity of HMTA and the micelles to collide with each other and thus may increase the length of the nanorods [21–23].

X-ray diffraction (XRD) is a well known technique for the structural identification and determination of the crystallite size. The XRD patterns of ZNRs thin films grown at different deposition times are presented in Fig. 1. All films exhibit a single peak along (002) plane at 52.11°, which could be attributed to the anisotropic growth of ZnO nanorods along [002] direction. The synthesized single crystalline nanorods lead to the formation of ZnO having a hexagonal wurtzite crystal structure (JCPDS 01-1136).

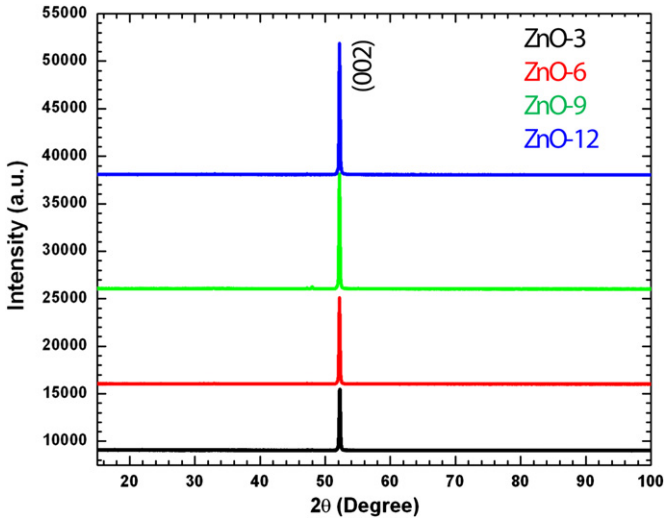


Fig. 1. XRD-spectra of ZnO samples (ZnO-3 to ZnO-12).

Fig. 2 shows the room temperature optical absorption spectra of the ZNRs films recorded in the wavelength range of 200–1100 nm without taking into account scattering and reflection losses. It is clearly seen that the absorbance decreases with an increase in wavelength, and a sharp decrease in absorbance near the band edge (390 nm) indicates better crystallinity of the films. The optical band gap ($E_g$) can be determined by the absorption coefficient ($\alpha$) and photon energy ($h\upsilon$) as follows:

$$\alpha = \alpha_0 \left( \frac{h\upsilon - E_g}{h\upsilon} \right)^n \quad (1)$$

where $\alpha_0$ is a constant, and the exponent '$n$' could have the values of 1/2, 3/2, 2 and 3, depending on the type of

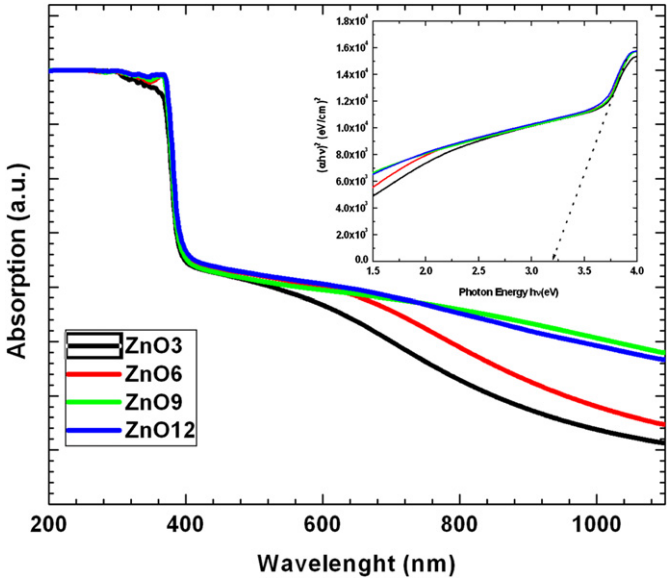


Fig. 2. Optical absorption spectra of ZnO thin film samples ZnO-3 to ZnO-12. Inset shows the variation of $(\alpha h\upsilon)^2$ versus $(h\upsilon)$ for ZnO-3 to ZnO-12 samples.

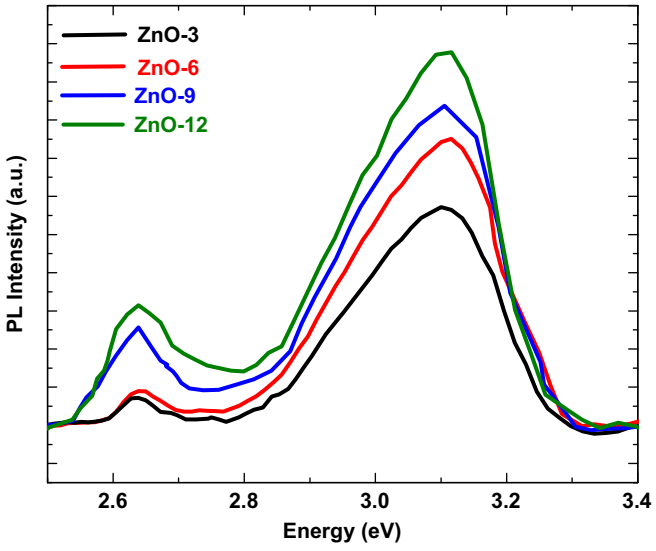


Fig. 3. PL spectra of ZnO samples ZnO-3 to ZnO-12.

electronic transition in the k-space. The value 1/2 corresponds to the direct band gap semiconductors. The variation of $(\alpha h\upsilon)^2$ vs $h\upsilon$ for all the films are shown in inset of Fig. 2. The nature of the plots indicates the existence of direct optical transition. The extrapolation of the straight line to zero absorption coefficient ($\alpha=0$) led to an estimate of the band gap energy ($E_g$) values and was found to be 3.2 eV.

Photoluminescence (PL) spectra of ZNRs with different rod lengths at room temperature were shown in Fig. 3. The

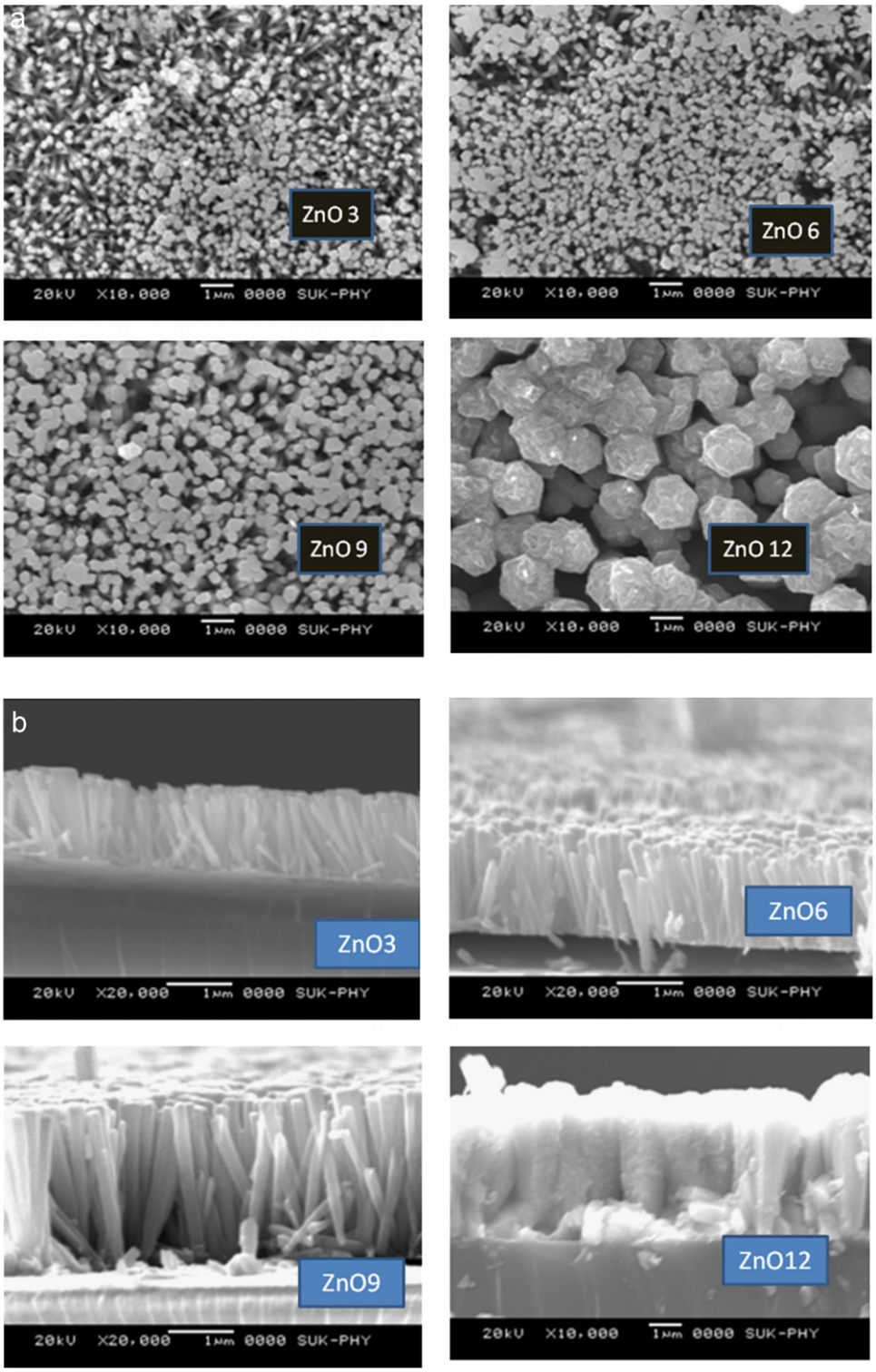


Fig. 4. (a) SEM images of ZnO thin films sample ZnO-3 to ZnO-12 (top view). (b) Cross-section SEM images of ZnO thin films sample ZnO-3 to ZnO-12. The nanorod length of ZnO-12 thin film sample is quite high compared to other nanorod arrays so the SEM image of ZnO-12 sample is reduced by a factor for better visibility of (b).

PL spectra of all the samples show two peaks as strong shoulder in ultraviolet (UV) and weak shoulder in the green region. The UV emission is due to the near band-edge free exciton transition from the localized level below the conduction band to the valance band. It was also observed that the intensity of the exciton emission depends on the degree of alignment of the ZnO nanorods. The photoluminescence spectra of all the ZnO nanorod samples show very strong emission at 3.22 eV. This strong absorption is generally attributed to the excitonic emission. Dev et al. [24] showed that the PL intensity of ZnO nanorods is much higher than ZnO thin film due to strong exciton emission in the rod compared to nanoparticles. The peak around 471 nm (2.63 eV) is due to the green emission that is commonly referred to as deep-level and trap state emission. The deep-level emission is mainly related to point defects, such as Zn interstitial and oxygen vacancies. Oxygen vacancies occur in three different charge states: the neutral oxygen vacancy, the singly ionized oxygen vacancy, and the doubly ionized oxygen vacancy. The singly ionized oxygen vacancy is so-called as luminescence centers [25]. However, this defect level emission was very weak in all the ZNRs samples. The UV emission shifts a little to 398 nm (3.11 eV) because of the ZnO nanostructures [26].

The morphology and size of ZNRs were characterized by SEM technique. It was found that the length/diameter aspect ratio increases as the reaction time prolongs (Fig. 4(a) and (b)). With an increase in deposition time, length of nanorods increases from 1.6 to 4.5 μm and spacing between them decreases from 180 to 100 nm. It was observed that the ZNRs with length more than 2.25 μm have a tendency to merge with neighboring nanorods which is clearly shown in Fig. 4(b). From the cross section images of ZnO nanorods (Fig. 4(b)) the aspect ratio was calculated. The aspect ratio gradually increases from 11.2 to 14.1 for the samples ZnO-3 to ZnO-9, while it decreased for the sample ZnO-12 (found to be 9.04). The decrease in the aspect ratio for the sample ZnO-12 is mainly due to increase in diameter. The length of nanorods and the spacing between them are an essential factor for light harvesting. The length of nanorods provides an effective surface area for light absorption and the spacing between them helps in light scattering and trapping. For the sample ZnO-3, the length of the nanorods is small as well as spacing between them is quite large. So the PEC performance of sample ZnO-3 is poor. However for the ZnO samples ZnO-6 and ZnO-9, the length as well as the spacing between them are adequate and are beneficial for PEC performance. An energy dispersive spectroscopic (EDS) analysis of the film (Fig. 5) shows that the products are mainly composed of Zn and O elements, which is consistent with the result of XRD.

Fig. 6 shows the *J–V* characteristics of ZnO-3 to ZnO-12 thin film samples. For all the samples, the *J–V* characteristic in the dark displays ideal diode-like rectifying characteristics for the fabricated PEC cells. Upon illumination, the *J–V* curves shift in the IV quadrant, indicating the generation of electricity, which is typical of solar cell characterization. The magnitude of the short circuit current

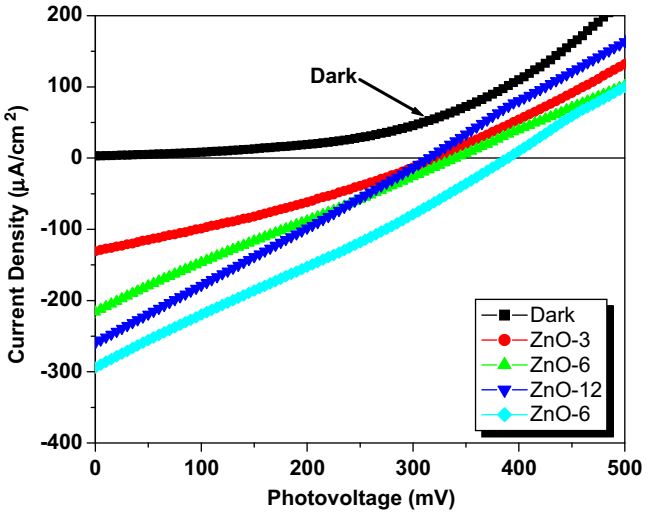


Fig. 6. *J–V* characteristics of ZnO nanorods thin film samples ZnO-3 to ZnO-12.

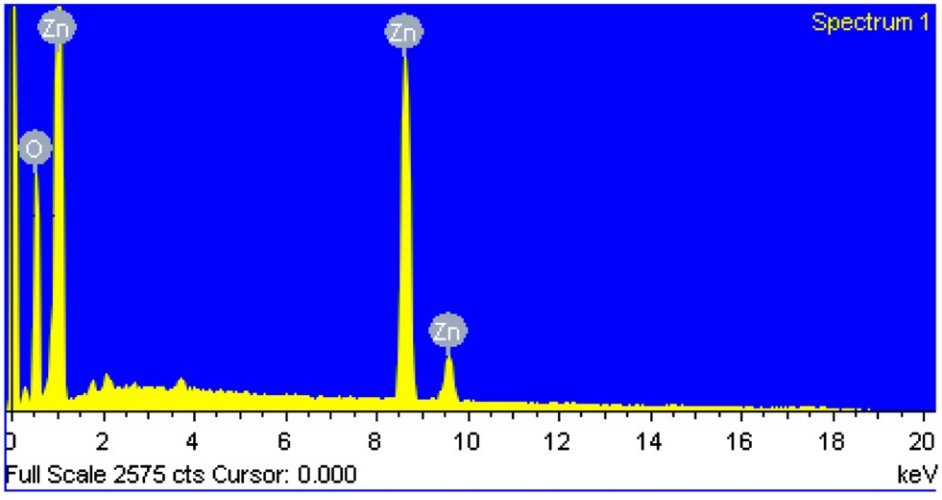


Fig. 5. EDS spectrum of ZnO-9 sample.

Table 1
Photovoltaic performance parameters of solar cells based on different ZNRs length.

| Sample | Rod Length | $J_{SC}$ (μA/cm$^2$) | $V_{oc}$ (mV) | $N_d$ | $R_s$ (Ω) | $R_{sh}$ (kΩ) | $V_{FB}$ (−V) | $FF$ | Efficiency ($\eta$) % |
|---|---|---|---|---|---|---|---|---|---|
| **ZnO-3** | 1.35 | 130 | 322 | 2.21 | 543 | 2.0 | 0.72 | 0.29 | 0.24 |
| **ZnO-6** | 1.65 | 217 | 340 | 2.97 | 625 | 1.6 | 0.74 | 0.23 | 0.34 |
| **ZnO-9** | 2.25 | 295 | 390 | 3.18 | 720 | 1.3 | 0.82 | 0.25 | 0.51 |
| **ZnO-12** | 4.50 | 260 | 313 | 3.42 | 812 | 1.2 | 0.71 | 0.22 | 0.40 |

density ($J_{SC}$) was found to be increased from 0.130, 0.217, 0.295 mA/cm$^2$ for ZnO-3, ZnO-6 and ZnO-9 samples respectively. However, it is found that $J_{SC}$ decreases suddenly up to 0.260 mA for ZnO-12 sample. The decrease in $J_{SC}$ value for the sample ZnO-12 may be due to minimum inter-space distance between nanorods which is clearly depicted in Fig. 4. Such compact ZnO layer constrains the charge separation between ZnO film and electrolyte interface. The detailed photovoltaic performance of ZnO with different nanorod lengths is summarized in Table 1. The open circuit voltage $V_{oc}$ was found to be increased from 322 to 392 mV with an increase in deposition time. The photovoltaic efficiency ($\eta$%) is calculated using the following equation:

$$\eta = \frac{V_{OC} I_{SC} FF}{P_{input}} \times 100 \tag{2}$$

where $I_{sc}$ is the short circuit current and $V_{oc}$ is the open circuit voltage, $P_{input}$ is the incident light energy, and $FF$ is the fill factor. The series resistance ($R_s$) and shunt resistance ($R_{sh}$) are estimated from the slope of the $I$–$V$ curves using the relation:

$$\left[\frac{dI}{dV}\right]_{I=0} \cong \frac{1}{R_s} \tag{3}$$

$$\left[\frac{dI}{dV}\right]_{V=0} \cong \frac{1}{R_{sh}} \tag{4}$$

Using a well known diode equation, junction ideality factor is calculated as

$$I = I_o e^{eV/nKT} \tag{5}$$

where $I$ is the forward current in dark, $I_o$ is the reverse saturation current, $V$ is the applied forward bias voltage and $n$ is the junction ideality factor. The ideality factors '$n$' was found to be 2.21, 2.97, 3.18 and 3.42 which increase with increasing deposition time. The ideality factor for all samples was found to be greater than 2 indicating that the recombination current is more. The higher value of '$n$' is an indication of the series resistance effect, surface states and the charge carrier recombination at the semiconductor–electrolyte interface.

The capacitance–voltage ($C$–$V$) measurements were performed for all samples and it provides useful information such as type of conductivity, width of depletion layer and flat band potential ($V_{fb}$). The flat band potential of a semiconductor gives information about the relative position of the Fermi levels in photoelectrode as well as the influence of electrolyte and charge transfer process across the junction. The $V_{fb}$ can be obtained by Mott–Schottky (M–S) relation using SCE as a reference electrode [27]:

$$C^2 = \frac{2}{q\varepsilon\varepsilon_0 N_d}\left(V - V_{fb} - \frac{KT}{q}\right). \tag{6}$$

where $\varepsilon_0$ is the permittivity of free space, $\varepsilon$ is the permittivity of the semiconductor electrode, $e$ is the charge on the carriers, and $N_d$ is the donor concentration, $T$ is the temperature of operation $\approx 300$ K, $K$ is Boltzmann's constant and $C$ is the space charge capacitance. The positive slope of the M–S plot confirms the n-type conductivity of the ZnO films. The intercept of the linear plot ($1/C^2 = 0$) was taken as the flat-band potential of the semiconductor at which band bending is zero. If we take the $V_{fb}$ as an approximation to the (quasi) Fermi level of an illuminated semiconductor, a PEC cell $V_{fb}$ potential should correlate with the cell's $V_{oc}$. In the present ZnO samples the increased open circuit voltage measured to the higher flat-band potential of ZnO-9 ($V_{fb}$) −0.82 V vs SCE as compared to that of ZnO-3 ($V_{fb}$) −0.72 V vs SCE.

## 4. Conclusion

ZnO thin films of different nanorod length have been successfully deposited by a simple and cost effective aqueous chemical route at low temperature. From XRD analysis it was observed that all ZnO samples exhibit hexagonal wurtzite crystal structure with the crystalline size varied from 37 to 49 nm. The increase in nanorods length from 1.6 μm to 4.5 μm with increase in deposition time was evidenced by cross-sectional SEM images. It is observed that the length of nanorods as well as inter-rod space distance plays a crucial role in the charge transport reaction enabling the improvement in light harvesting properties.

## Acknowledgment

One of the authors SSM wishes to acknowledge the DAE-BRNS Mumbai for financial support through the DAE-BRNS Project no. 2008/37/8/BRNS/1489 for the 2008–2012.

## References

[1] Z.L. Wang, X.Y. Kong, Y. Ding, P. Gao, W.L. Hughes, R. Yang, Y. Zhang, Advanced Functional Materials 14 (2004) 943.
[2] M. Breedon, M.B. Rahmani, S.H. Keshmiri, W. Wlodarski, K.K. Zadeh, Materials Letters 64 (2010) 291.

[3] H. Usui, Materials Letters 63 (2009) 1489.
[4] F. Xu, Y. Lu, Y. Xie, Y. Liu., Vacuum 83 (2009) 360.
[5] J. Qiu, X. Li, W. Yu, X. Gao, W. He, S.J. Park, Thin Solid Films 517 (2008) 626.
[6] Y. Chen, D.M. Bagnall, H.J. Koh, K.T. Park, K. Hiraga, Z. Zhu, T. Yao, Journal of Applied Physics 84 (1998) 3912.
[7] L. Yanbo, Z. Maojun, L. Ma, M. Zhong, W. Shen, Inorganic Chemistry 47 (2008) 3140.
[8] A.I. Inamdar, S.H. Mujawar, S.B. Sadale, A.C. Sonavane, M.B. Shelar, P.S. Shinde, P.S. Patil, Solar Energy Materials and Solar Cells 91 (B) (2007) 865.
[9] B. Ismail, M.A. Abaab, B. Rezig, Thin Solid Films 383 (2001) 92.
[10] M.A. Martinez, J. Herrero, M.T. Gutierrez, Solar Energy Materials and Solar Cells 45 (1997) 75.
[11] S.A. Vanalakar, R.C. Pawar, M.P. Suryawanshi, S.S. Mali, D.S. Dalavi, A.V. Moholkar, K.U. Sim, Y.B. Kown, J.H. Kim, P.S. Patil, Materials Letters 65 (2011) 548.
[12] R.C. Pawar, J.S. Shaikh, P.S. Patil, Materials Today 14 (2011) 447.
[13] H. Sato, T. Minami, T. Miyata, S. Takata, M. Ishii, Thin Solid Films 246 (1994) 65.
[14] N.L. Tarwal, P.R. Jadhav, S.A. Vanalakar, S.S. Kalagi, R.C. Pawar, J.S. Shaikh, S.S. Mali, D.S. Dalavi, P.S. Shinde, P.S. Patil, Powder Technology 208 (2011) 185.
[15] A. Ennaoui, M. Weber, R. Scheer, H.J. Lewerenz, Solar Energy Materials and Solar Cells 54 (1998) 277.
[16] M. Izaki, T. Omi, Applied Physics Letters 68 (1996) 2439.
[17] L. Vayssieres, K. Keis, S. Lindquist, A. Hagfeldt, Journal of Physical Chemistry B 10 (5) (2001) 3350.
[18] D.S. Boyle, G.K. Ovender, P. O'Brien, Chemical Communications (2002) 80.
[19] M. Law, L.E. Greene, J.C. Johnson, R. Saykally, P. Yang, Nature Materials 4 (2005) 455.
[20] S. Baruah, J. Dutta, Science and Technology of Advanced Materials 10 (2009) 013001.
[21] S. Yue, J. Lu, J. Zhang, Materials Letters 63 (2009) 2149.
[22] L. Liao, D.H. Liu, J.C. Li, C. Liu, Q. Fu, M.S. Ye, Applied Surface Science 240 (2005) 175.
[23] Z.L. Wang, Materials Today 7 (2004) 26.
[24] A. Dev, S. Chaudhuri, B.N. Dev, Bulletin of Materials Science 31 (3) (2008) 551.
[25] H.S. Kang, J.S. Kang, J.W. Kim, S.Y. Lee, Journal of Applied Physics 95 (2004) 1246.
[26] X.D. Wang, Y. Ding, C.J. Summers, Z.L. Wang, Journal of Physical Chemistry B 108 (2004) 8773.
[27] L. Djellal, A. Bouguelia, M. Trari, Materials Chemistry and Physics 109 (2008) 99.